Inorg. Chem. **2006**, *45*, 10938–10946

Magnetic Structure and Magnetic Properties of Synthetic Lindgrenite, $Cu_3(OH)_2(MoO_4)_2$

Serge Vilminot,*,† Gilles André,‡ Mireille Richard-Plouet,§ Françoise Bourée-Vigneron,‡ and Mohamedally Kurmoo*,#

Groupe des Matériaux Inorganiques, IPCMS, CNRS-ULP UMR7504, 23 rue du Loess, BP 43, 67034 Strasbourg Cedex 2, France, Laboratoire Léon Brillouin, CEA-CNRS, CEA Saclay, 91191 Gif-sur-Yvette Cedex, France, Institut des Matériaux Jean Rouxel, Laboratoire de Chimie des Solides, 2 rue de la Houssinière, BP 32229, 44322 Nantes Cedex, France, and Laboratoire de Chimie de Coordination Organique, CNRS-UMR7140, Tectonique Moléculaire du Solide, Université Louis Pasteur, Institut Le Bel, 4 rue Blaise Pascal, 67000 Strasbourg Cedex 01, France

Received June 28, 2006

Synthetic $Cu_3(OH)_2(MoO_4)_2$ consists of $Cu_3(OH)_2$ brucite ribbons of edge-sharing copper octahedra connected by MoO_4 into a 3D network as in the mineral, lindgrenite, for all temperatures between 1.5 and 300 K. Each ribbon consists of a triangular connection between two different types of copper atom (Cu(1) and 2 Cu(2)) via μ_3-OH. The MoO_4 acts both as one- and three-atom bridges to connect six Cu atoms belonging to three adjacent ribbons. The magnetic properties are consistent with those of ferrimagnetic chains, and the resulting moment of each chain is parallel below the long-range magnetic ordering at 13 K. The Curie constant is 0.468(1) emu K mol^{-1} of Cu; the Weiss temperature is –14.2(2) K, and the saturation magnetization at 2 K in 50 kOe is 0.41 N μ_B mol^{-1} of Cu. Analyses of the neutron powder diffraction reveal an ordered magnetic state where the moment of Cu(1) is antiparallel to those of the two Cu(2); all of them point along the *a* axis without any sign of geometrical frustration. Any degeneracy that may be present because of the triangular topology of the Cu atoms ($s = 1/2$) appears to be lifted by the distortion from an ideal equilateral geometry of the triangle. The entropy, estimated from the heat capacity measurements, attains 50% of the total of 17.7 J K^{-1} mol^{-1}, close to that expected for three Cu atoms ($3R$ ln 2), up to the long range ordering temperature, and the remaining is associated with the low dimensionality of the material.

Introduction

Synthetic routes for organic, inorganic, and metal−organic materials using the hydrothermal technique are being developed for academic research purposes, as well as for large-scale industrial production.[1] The ease of these syntheses at modest temperatures, pressures, and also, costs makes the technique very appealing. We and other researchers have been involved in reproducing the temperature and pressure conditions usually involved in the elaboration of synthetic minerals.[2−4] The preparation of the synthetic compounds appears interesting when studying the magnetic properties since the stoichiometry and purity can be controlled, whereas

* To whom correspondence should be addressed. Telephone: 00 33 3 88 10 71 28. Fax: 00 33 3 88 10 72 47. Email: vilminot@ipcms.u-strasbg.fr (S.V.). Telephone: 00 33 3 90 24 13 56. Fax: 00 33 3 90 24 13 25. Email: kurmoo@chimie.u-strasbg.fr (M.K.).

† IPCMS, Strasbourg.

‡ Laboratoire Léon Brillouin, Gif-sur-Yvette.

§ Institut des Matériaux Jean Rouxel, Nantes.

Université Louis Pasteur, Strasbourg.

(1) (a) Cundy, C. S.; Cox, P. A. *Chem. Rev.* **2003**, *103*, 663−701 and references therein. (b) Barrer, R. M. *Hydrothermal Chemistry of Zeolites*; Academic Press: London, 1982. (c) Rabeneau, A. *Angew. Chem., Int. Engl.* **1985**, *24*, 1026.

(2) (a) Vilminot, S.; Richard-Plouet, M.; André, G.; Swierczynski, D.; Bourée-Vigneron, F.; Marino, E.; Guillot, M. *Cryst. Eng.* **2002**, *5*, 177. (b) Vilminot, S.; Richard-Plouet, M.; André, G.; Swierczynski, D.; Guillot, M.; Bourée-Vigneron, F.; Drillon, M. *J. Solid State Chem.* **2003**, *170*, 255. (c) Vilminot, S.; Richard-Plouet, M.; André, G.; Swierczynski, D.; Bourée-Vigneron, F.; Kurmoo, M. *Dalton Trans.* **2006**, 1455−1462. (d) Ben, Salah, M.; Vilminot, S.; André, G.; Richard-Plouet, M.; Bourée-Vigneron, F.; Mhiri, T.; Kurmoo, M. *Chem.—Eur. J.* **2004**, *10*, 2048. (e) Ben Salah, M.; Vilminot, S.; Mhiri, T.; Kurmoo, M. *Eur. J. Inorg. Chem.* **2004**, 2272. (f) Vilminot, S.; Richard-Plouet, M.; André, G.; Swierczynski, D.; Bourée-Vigneron, F.; Kurmoo, M. *Inorg. Chem.* **2003**, *42*, 6859. (g) Ben Salah, M.; Vilminot, S.; André, G.; Richard-Plouet, M.; Mhiri, T.; Takagi, S.; Kurmoo, M. *Chem. Mater.* **2005**, *17*, 2612. (h) Ben Salah, M.; Vilminot, S.; André, G.; Richard-Plouet, M.; Bourée-Vigneron, F.; Mhiri, T.; Kurmoo, M. *J. Am. Chem. Soc.* **2006**, *128*, 7972.

10.1021/ic061182m CCC: $33.50
Published on Web 12/01/2006

the minerals may contain different transition metals.[2−5] In many cases, the synthetic equivalents of minerals have been obtained, but nature appears to be an excellent, and even better, laboratory since many of the natural minerals have so far not been reproduced. For instance, the anhydrous copper hydroxysulfates, such as $Cu_3(OH)_4SO_4$, antlerite, and $Cu_4(OH)_6SO_4$, brochantite, can be easily prepared by hydrothermal synthesis.[2] However, the syntheses of the hydrated minerals, such as $Cu_4(OH)_6SO_4(H_2O)_2$, langite, posnjakite, and wroewolfeite,[6−8] and $Cu_7(OH)_{10}(SO_4)_2(H_2O)_3$, schulenbergite, have not been successful at the laboratory level.[9] All the hydrated phases and brochantite exhibit a structure build up of brucite-like sheets of distorted octahedral copper. In contrast, antlerite contains triple chains of copper octahedra. In addition to the preparation of known phases, it is possible to replace some of the components or even functionalize the minerals with organic or inorganic moieties with specific properties.[10−12] For example, the substitution of sulfate by selenate allows one to obtain the compounds corresponding to antlerite and brochantite,[11,12] even if there are no natural equivalents. Among other tetrahedral anions, molybdate is known to form basic salts of copper (i.e., szecnicsite, $Cu_3(OH)_4MoO_4$, and lindgrenite, $Cu_3(OH)_2(MoO_4)_2$).[13,14] Again, the hydrothermal synthesis we performed does not yield the formation of szecnicsite but, instead, produces lindgrenite in a wide spectrum of starting compositions and for different temperatures. Szecnicsite is not isostructural to antlerite, but it contains similar triple chains of edge-shared copper octahedra. Therefore, it would have been of interest to compare the corresponding magnetic properties. On the other hand, lindgrenite also contains chains of edge-shared copper octahedra, with the alternating succession of one then two copper octahedra along the ribbons. The related structure appears interesting from a magnetic point of view, similar to that we experienced for a similar cobalt ribbon in $Co_3(OH)_2(C_4O_4)_2{\cdot}3H_2O$.[15] Such systems have been of recent interest in the physics community, and the physicists describe them as linear chain distorted diamonds.[16] Moreover, a triclinic modification has been shown[17] that differs from the usual monoclinic form in that the ribbons are now parallel to each other rather than being arranged in a herringbone fashion, as for lindgrenite.

In their ongoing studies to understand the magnetism of geometrically frustrated systems, Shores et al. have recently reported the synthesis of lindgrenite and two other forms that were elegantly modified by bipyridine and piperazine.[3,10] The two ditopic ligands, interestingly, break the inorganic 3D network into layers, consequently transforming the ferromagnetic lindgrenite into antiferromagnets with a critical metamagnetic field of 2 kOe. Although the Weiss constant of lindgrenite is negative and the saturation magnetization is only ∼1/3 of that expected for a ferromagnet, it was described as a ferromagnet. They propose a model-of-spin arrangement, where only the spins within one chain were considered, to explain the observation of metamagnetism in the organic-modified forms.[10]

Other interest in materials containing molybdenum oxide is the result of their promising applications in the area of catalysis, sorption, electrical conductivity, magnetism, photochemistry, sensors, and energy storage.[18−22] However, the majority of these studies are concerned with compounds like $FeMoO_4$ and $Fe_2(MoO_4)_3$ for the synthesis of formaldehyde or Fe−Mo−O catalysts for the oxidation of toluene to benzaldehyde,[23] $NiMoO_4$[24] or Cu, Mn, and Co molybdates[25] for the oxidative dehydrogenation of propane, and $Cu_3Mo_2O_9$ for catalytic deep oxidation (combustion) of the emitted harmful gases (e.g., CO, NO, and hydrocarbons).[26] Interestingly, lindgrenite has been considered for smoke suppression and fire retardation of poly(vinyl chloride).[27]

Here, we present the hydrothermal synthesis of the hydrogenated and deuterated analogues of lindgrenite, their thermal and optical properties, and magnetic properties as a function of temperature and field. We also report the magnetic structure obtained from neutron powder diffraction and the heat capacity in zero field. All results point to a

(3) (a) Nocera, D. G.; Bartlett, B. M.; Grohol, D.; Papoutsakis, D.; Shores, M. P. *Chem.—Eur. J.* **2004**, *10*, 3850 and references therein. (b) Wills, A. S. *Phys. Rev. B.* **2001**, *63*, 064430. (c) Shores, M. P.; Nytko, E. A.; Bartlett, B. M.; Nocera, D. G. *J. Am. Chem. Soc.* **2005**, *127*, 13462.
(4) Harrison, A. *J. Phys: Condens. Matter* **2004**, *16*, S553.
(5) (a) Hawthorne, F. C.; Krivovichev, S. V.; Burns, P. C. *Rev. Mineral.* **2000**, *40*, 1. (b) Eby, R. K.; Hawthorne, F. C. *Acta Crystallogr.* **1993**, *B49*, 28.
(6) Galy, J.; Jauf, J.; Pulou, R.; Sempere, R. *Bull. Minéral.* **1984**, *107*, 641−648.
(7) Mellini, M.; Merlino, S. *Z. Kristallogr.* **1979**, *149*, 249−257.
(8) Hawthorne, F. C.; Groat, L. A. *Am. Mineral.* **1985**, *70*, 1050−1055.
(9) Mumme, W. G.; Sarp, H.; Chiappero, P. J. *Arch. Sci. Geneve* **1994**, *47*, 117−124.
(10) Shores, M. P.; Bartlett, B. M.; Nocera, D. G. *J. Am. Chem. Soc.* **2005**, *127*, 17986−17987.
(11) Giester, G.; *Monatsh. Chem.* **1991**, *122*, 229−234.
(12) Lachenal, G.; Vignalou, J. *Thermochim. Acta* **1987**, *111*, 195.
(13) (a) Stolz, J.; Armbruster, T. *Neues Jahrb. Mineral., Monatsh.* **1998**, 278−288. (b) Francis, C. A.; Pitman, L. C.; Lange, D. E. *Mineral. Rec.* **1997**, *28*, 387−394.
(14) (a) Hawthorne, F. C.; Eby, R. K. *Neues. Jahrb. Mineral., Monatsh.* **1985**, *5*, 234−240. (b) Calvert, L. D.; Barnes, W. H. *Can. Mineral.* **1957**, *6*, 31−51. (c) Barnes, W. H. *Am. Mineral.* **1949**, 34, 163−172. (d) Palache, C. *Am. Mineral.* **1935**, 20, 484−91.
(15) Kurmoo, M.; Kumagai, H.; Chapman, K. W.; Kepert, C. J. *Chem. Commun.* **2005**, 3012−3014.
(16) (a) Okamoto, K.; Tonegawa, T.; Kaburagi, M. *J. Phys. Condens. Matter* **2003**, *15*, 5979−5995. (b) Kikuchi, H.; Fujii, Y.; Chiba, M.; Mitsudo, S.; Idehara, T.; Tonegawa, T.; Okamoto, K.; Sakai, T.; Kuwai, T.; Ohta, H. *Phys. Rev. Lett.* **2005**, *94*, 227201.
(17) Xu, Y.; Lu, J.; Goh, N. K. *J. Mater. Chem.* **1999**, *9*, 1599−1602.
(18) Chippindale, A. M.; Cheetham, A. K. In *Studies in Inorganic Chemistry*; Elsevier: Amsterdam, 1994; Vol. 19, pp 1146−184 and references therein.
(19) Johnson, L. F.; Boyd, G. D.; Nassau, K.; Sode, R. R. *Phys. Rev.* **1962**, *126*, 1406.
(20) Bruce, D. W.; Hare, D. O. *Inorganic Materials*; Wiley: Chichester, U.K.; 1992.
(21) Bein, T., Ed. *Supramolecular Architecture: Synthetic Control in Thin Films and Solids*; ACS Symposium Series 499; American Chemical Society: Washington, DC, 1992.
(22) Cheetham, A. K. *Science* **1994**, *264*, 794 and references therein.
(23) Zhang, H.; Shen, J.; Ge, X. *J. Solid State Chem.* **1995**, *117*, 127−135.
(24) Mazzochia, C.; Aboumrad, C.; Diagne, C.; Tempesti, E.; Herrman, J. M.; Thomas, G. *Catal. Lett.* **1991**, *10*, 181.
(25) Palacio, L. A.; Echavarria, A.; Sierra, L.; Lombardo, E. A. *Catal. Today* **2005**, *107−108*, 338−345.
(26) Hasan, M. A.; Zaki, M. I.; Kumari, K.; Pasuputely, L. *Thermochim. Acta* **1998**, *320*, 23−32.
(27) Starnes, W. H., Jr; Pike, R. D.; Cole, J. R.; Doyal, A. S.; Kimlin, E. J.; Lee, J. T.; Murray, P. J.; Quinlan, R. A.; Zhang, J. *Polym. Degrad. Stab.* **2003**, *82*, 15−24.

ferrimagnetic ground state below 13 K without any sign of geometrical frustration.

Experimental Section

Preparation of $Cu_3(OH)_2(MoO_4)_2$. Synthetic lindgrenite, $Cu_3(OH)_2(MoO_4)_2$ (**1**), was obtained using an approach similar to that of Clearfield et al.,[28] via the hydrothermal reaction of copper nitrate hemipentahydrate, $Cu(NO_3)_2 \cdot 2.5H_2O$ (Aldrich, 98%), sodium molybdate dihydrate, $Na_2MoO_4 \cdot 2H_2O$ (Aldrich, 99.5%), and sodium hydroxide, NaOH (Prolabo, 97%), at 220 °C for 48 h. Copper nitrate (12.9 mmol, 3.05 g) and sodium molybdate (8.6 mmol, 2.08 g) were separately dissolved in 15 mL of water. The solutions were mixed to give an amorphous light-green precipitate. Sodium hydroxide (8.6 mmol, 0.34 g) dissolved in 10 mL of water was then added, yielding a color change to yellow-green. The suspension was poured into Teflon-lined stainless steel bombs (125 cm^3), filled to ~1/3, and heated at 220 °C for 2 days. The powder was filtered and then washed with water, followed by acetone, before being dried at 40 °C in air. XRPD indicates a pure sample where all the peaks were indexed to those of lindgrenite. Anal. Calcd for $H_2O_{10}Cu_3Mo_2$: Cu, 35.01; Mo, 35.24%. Found: Cu, 35.9; Mo, 35. 4%.

A Sample of $Cu_3(OD)_2(MoO_4)_2$ (**2**) for powder neutron diffraction studies was prepared using the same synthetic procedure by replacing H_2O with heavy water, D_2O, to replace as much H as possible with D in the samples. Deuterium reduces the intense background usually observed for H samples which results from the high incoherent scattering factor of hydrogen. The powder was filtered; then, it was washed with a small amount of heavy water, followed by acetone, before being dried at 40 °C in air. Upon Rietveld refinement of the neutron diffraction data, we realized that the sample was contaminated with ~3% $Na_2MoO_4 \cdot 2D_2O$, possibly because of inadequate washing with heavy water.

Characterization. Thermal analyses were performed using a TA-STD-Q600 apparatus at a 5 °C min^{-1} heating rate under air. Infrared spectra were recorded with a Digilab FTS3000 spectrometer by transmission through KBr pellets containing 1% of the powder. Powder X-ray diffraction patterns were recorded using a D5000 Siemens diffractometer equipped with a forward monochromator (Cu $K\alpha_1$, 1.5406 Å).

The neutron diffraction experiments were performed at the Laboratoire Léon Brillouin (CEA Saclay) using the 3T2 and G4.1 diffractometers. Data obtained on the high-resolution powder diffractometer 3T2 ($\lambda = 1.2252$ Å, $6° < 2\theta < 126°$) were used for the refinement of the nuclear structure at 300 K, and those from the multidetector (800 cells) G4.1 ($\lambda = 2.4266$ Å) were used for the determination of the magnetic structure and the thermal evolution study of the low-temperature patterns. Therefore, 10 diffraction patterns were recorded in the 2θ range of 11−90.9° at different temperatures between 1.5 and 18 K. The powder sample was placed in a cylindrical vanadium container and held in a liquid helium cryostat. Nuclear and magnetic structures were refined using the FULLPROF program.[29] The nuclear scattering lengths ($b_{Cu} = 0.7718 \times 10^{-12}$ cm, $b_{Mo} = 0.6715 \times 10^{-12}$ cm, $b_O = 0.5803 \times 10^{-12}$ cm, $b_D = 0.6671 \times 10^{-12}$ cm, and $b_H = -0.3739 \times 10^{-12}$ cm) and copper magnetic form factors were included in this program.

Magnetization measurements were performed in the range of 2−300 K and in a field of ±50 kOe with a Quantum Design MPMS-XL SQUID magnetometer; ac susceptibility was determined in the same apparatus in an applied field of 3.5 Oe, oscillating at 20 Hz. Specific-heat measurements were carried out in a home-built apparatus employing a quasi-adiabatic method in the temperature range of 1.6−37 K.

Results and Discussion

Synthesis. Although our original aim was to study the two minerals, lindgrenite and szenicsite,[13] as a comparative work and with antlerite because of their slightly different structures, we have so far not succeeded in obtaining szenicsite. We tried to prepare szenicsite, $Cu_3(OH)_4MoO_4$, using the same procedure described in the Experimental Section and by varying the experimental conditions. The conditions described in the experimental section principally produce lindgrenite with a yield of ~90%, and XRD reveals the presence of a single phase. However, other phases have been identified under slightly different conditions. When the stoichiometric proportion Cu/Mo/NaOH is 3:2:2 pure lindgrenite results; the concomitant formation of $NaCu(OH)MoO_4$ as a very minor phase is detected if the amount of NaOH is decreased to 1.5 and 1. In the presence of an excess MoO_4^{2-}, Cu/Mo/NaOH = 3:3:1−3, a gray or black precipitate is obtained, where XRD reveals a mixture of lingrenite and CuO or pure CuO. This result may be related to the increase of pH promoted by the excess of $Na_2MoO_4 \cdot 2H_2O$. In the presence of a low concentration of MoO_4^{2-}, Cu/Mo/NaOH = 3:0.5−1.5:0.5−1.5, pure lindgrenite is obtained for low concentrations of NaOH, and the concomitant formation of $NaCu(OH)MoO_4$ is shown for higher concentrations. The starting copper salt, together with control of the alkalinity, is important. We tried several experiments in which we substituted copper sulfate for copper nitrate. If NaOH is also used, we always get CuO. Subsequently, experiments were performed without NaOH. Lindgrenite is obtained for Cu/Mo = 3:2.5−4.5, where the excess of $Na_2MoO_4 \cdot 2H_2O$ is necessary to increase the pH value. For Mo contents higher than 4.5, $NaCu(OH)MoO_4$ is obtained as dark-green single crystals. For all the above synthetic procedures, the temperature must be restricted to 220 °C; higher temperature always results in the formation of copper oxide. The slight differences for the two starting materials may be related to the respective pH values of copper nitrate and copper sulfate solutions, the first one being more acidic.

Our procedure described above is closely related to those in the literature.[27−28] Synthetic lindgrenite was previously obtained either by reflux overnight of a pale blue-green aqueous suspension obtained by dropwise addition of a $Na_2MoO_4 \cdot 2H_2O$ solution to a copper sulfate(I)[10,27,28] or by hydrothermal treatment of MoO_3 and CuO in an aqueous $Na_2MoO_4 \cdot 2H_2O$ solution at 200 °C[30] or of an aqueous suspension obtained from $(NH_4)_6Mo_7O_{24} \cdot 4H_2O/CuCl_2 \cdot 2H_2O$/2-ampy at 180 °C for 2 days (2-ampy = 2-aminopyridine).[31]

X-ray Powder Diffraction. X-ray diffraction data collected on the pale green powder indicate a highly crystalline

(28) Clearfield, A.; Moini, A.; Rudolf, P. R. *Inorg. Chem.* **1985**, *24*, 4606−4609.
(29) Rodriguez-Carvajal, J. *FULLPROF: Rietveld, profile matching and integrated intensity refinement of X-ray and/or neutron data*, version 3.5d; Léon-Brillouin Laboratory: CEA Saclay, France, 1998.
(30) Moini, A.; Peascoe, R.; Rudolf, P. R.; Clearfield, A. *Inorg. Chem.* **1986**, *25*, 3782−3785.
(31) Pavani, K.; Ramanan, A. *Eur. J. Inorg. Chem.* **2005**, 3080−3087.

materials, and indexing of the peaks confirmed the presence of only lindgrenite, $Cu_3(OH)_2(MoO_4)_2$ (JCPDS file 86-2311). All the Bragg reflections have been indexed using the pattern matching module of the FULLPROF program yielding the unit cell parameters $a = 5.6139(1)$ Å, $b = 14.0287(3)$ Å, $c = 5.3972(1)$ Å, and $\beta = 98.496(1)°$, confirming that the sample is single phase.[31] Figure S1 (Supporting Information) gives the corresponding experimental and calculated diffractograms.

Thermal Analysis. The TGA (Figure S2) recorded under a flow of air reveals a weight loss between around 370 and 410 °C. It corresponds to the departure of OH groups as H_2O, $\Delta P_{obsd}/P = 3.27\%$, $\Delta P_{calcd}/P = 3.34\%$. The X-ray diffraction pattern recorded on the sample, having a red color, obtained after this weight loss reveals the formation of $Cu_3Mo_2O_9$ in agreement with JCPDS file 24-55. This agreement between calculated and observed weight loss and the content of the residual compound, $Cu_3Mo_2O_9$, having the same stoichiometry as lindgrenite, confirms the purity of **1**. A second weight loss takes place between around 840 and 895 °C and is related to the decomposition of $Cu_3Mo_2O_9$ into unidentified oxides.

Infrared Spectroscopy. The IR spectrum recorded between 300 and 4000 cm^{-1} on **1** reveals three families of vibrational bands centered around 3350, 850, and 440 cm^{-1}. As the first one is shifted in the spectrum of **2**, it can be attributed to the symmetric and antisymmetric stretching modes of the O−H bonds. In **2**, these bands appear at around 2500 cm^{-1} [i.e., a ratio of 0.75 which is close to the expected value of $\sqrt{(18/(2 \times 17))}$]. Between 960 and 820 cm^{-1}, four bands (one broad, two sharp. and one shoulder) are observed for **1** and **2**. The ν_1 and ν_3 modes of the molybdate ion are expected in this region, where $\nu_1 = 897$ cm^{-1} and $\nu_3 = 837$ cm^{-1} were observed for the free ion in solution.[32] Because of the C_1 local symmetry, the number of infrared active vibrations increases to 3 for ν_3, and ν_1 becomes infrared active. Because the relative intensities of the bands between 960 and 820 cm^{-1} do not significantly vary between **1** and **2**, they have been attributed to MoO_4^{2-} vibrations. We propose the assignment of the 958 cm^{-1} band to $\nu_1(MoO_4)$ and the 914, 868, and 825 cm^{-1} bands to $\nu_3(MoO_4)$ in agreement with the proposed assignment of ν_1 at the highest wavenumber.[32] These bands appear at 952, 911, 865, and 831 cm^{-1} for the deuterated sample, while only the last three are observed for $Na_2MoO_4{\cdot}2H_2O$ possibly because of the higher symmetry of the MoO_4. The spectrum of **2** reveals two additional sharp bands at 671 and 635 cm^{-1} that have been attributed to the libration modes. Therefore, the corresponding O−H bands are expected in the same regions as those of MoO_4^{2-}; the O−H libration bands probably being unresolved, are hidden by the broad band at 825 cm^{-1}.[32] The five bands between 460 and 300 cm^{-1} have been attributed to (a) Cu−OH(D) vibration bands at 455 and 440 cm^{-1} for **1** and **2**, respectively, the slight shift toward lower energies for **2** being in agreement with the mass difference (such a band is not shown in the IR spectrum recorded under the same conditions on $Na_2MoO_4{\cdot}2H_2O$), (b) to O−H vibration at 420 cm^{-1} since this band nearly disappears for **2**, and (c) to ν_2 and $\nu_4(MoO_4)$ for the bands at 387, 352, and 341 cm^{-1}, their positions being the same for **1** and **2**. The results are summarized in Table S1 and Figure S3 (Supporting Information).

(32) (a) Frost, R. L.; Duong, L.; Weier, M. *Neues. Jahrb. Mineral.* **2004**, *180*, 245−260. (b) Nakamoto, K. *Infrared and Raman Spectra of Inorganic and Coordination Compounds*; John Wiley: New York, 1986. (c) Weinstock, N.; Schulze, H.; Müller, A. *J. Chem. Phys.* **1973**, *59*, 5063−5067.

Table 1. Summary of the Neutron Powder Diffraction Data Analyses for Nuclear and Magnetic Structures

	300 K	1.5 K
a (Å)	5.3980(2)	5.4052(2)
b (Å)	14.0234(4)	14.0716(5)
c (Å)	5.6129(2)	5.6183(2)
β (deg)	98.497(2)	98.745(2)
V (Å^3)	420.22(5)	422.36(6)
Z	2	2
space group	$P2_1/n$	$P2_1/n$
wavelength (Å)	1.2244	2.4266
2θ range, step	6.08−120.63°, 0.05°	11.0−90.9°, 0.1°
reflns (nuclear)	1310	99
reflns (magnetic)		197
params	45	39
R_P (%)	5.34	7.27
R_{WP} (%)	6.26	8.41
R_B (%)	1.49	2.00
R_F (%)	0.70	1.64
$R_{magnetic}$ (%)		4.99
GOF	2.04	

Table 2. Final Atomic Positions from Neutron Powder Diffraction Data at 300 K

atom[a]	x/a	y/b	z/c	B (Å)	occupation
Cu1	0	0	0	0.88(5)	2.0
Cu2	0.8659(4)	0.0947(2)	0.4881(4)	0.96(4)	4.0
Mo	0.4559(4)	0.1547(2)	0.8763(4)	0.54(3)	4.0
O1	0.9805(6)	0.2226(2)	0.4412(5)	1.11(5)	4.0
O2	0.6541(6)	0.0928(2)	0.1000(5)	1.29(5)	4.0
O3	0.5543(6)	0.1307(2)	0.5948(5)	1.28(5)	4.0
O4	0.1447(6)	0.1143(2)	0.8767(5)	1.04(5)	4.0
OD	0.1378(6)	0.0311(2)	0.3448(5)	1.08(5)	4.0
H	0.2874(6)	0.0684(2)	0.3724(6)	1.46(6)	0.36(3)
D	0.2874(6)	0.0684(2)	0.3724(6)	1.46(6)	3.64(3)

[a] D/(H + D) = 0.91.

Nuclear Structure Description. Although the nuclear structure of the natural mineral is known, it is important for this work to show that the synthetic analogue has the same structure at all temperatures, as well as establish the hydrogen positions precisely from the neutron data. Therefore, the nuclear structure has been refined (Tables 1 and 2) from the neutron powder data collected at room temperature on the high-resolution 3T2 diffractometer and from the X-ray powder diffraction starting from the atomic coordinates reported by Hawthorne and Eby (Figure S4).[14] A good agreement with the X-ray single-crystal results is observed in both cases. Three very weak lines of the G4.1 neutron data were not indexed and have been attributed to the presence of a small amount of sodium molybdate, $Na_2MoO_4{\cdot}2D_2O$. It was not observed by X-ray diffraction, and it amounts to around 3% according to the refinement. The inclusion of its contribution in the refinement through the pattern-matching procedure results in a better convergence.

As the main features of the structure are already reported,[14]

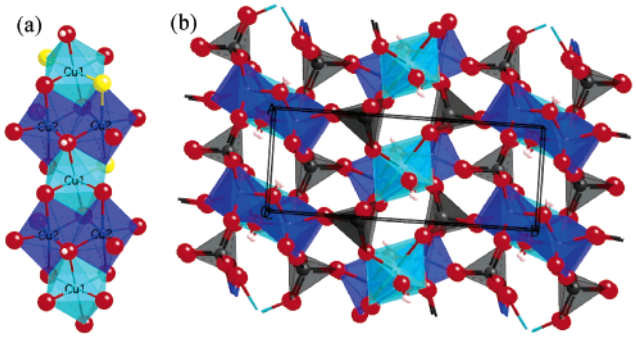

Figure 1. (a) View of a single ribbon showing the edge-sharing copper octahedra where the long bonds characterizing the Jahn−Teller distortions are highlighted by yellow oxygen atoms and (b) a projection of the structure along the ribbons (*c* axis) showing the herringbone arrangement and the connection of the ribbons by the MoO_4.

Table 3. Selected Interatomic Distances (Å) at 300 K

Cu1−O2	2.409(3) (×2)	Cu2−O1	1.928(4)
Cu1−O4	1.953(3) (×2)	Cu2−O2	2.306(3)
Cu1−OD	2.016(3) (×2)	Cu2−O3	1.934(4)
<Cu1−O>	2.126	Cu2−O4	2.476(3)
Mo−O1	1.760(4)	Cu2−OD	1.986(4)
Mo−O2	1.754(4)	Cu2−OD	1.999(4)
Mo−O3	1.772(4)	<Cu2−O>	2.105
Mo−O4	1.774(4)	OD−D	0.956(4)
<Mo−O>	1.765	D···O3	1.966(4)

we will only highlight some of the features relevant to the magnetism and magnetic structure discussed below. The key feature of the structure of lindgrenite is the presence of $Cu_3(OH)_2$ ribbons (Figure 1a) of the brucite structure consisting of edge-sharing copper octahedra running parallel to the *c* axis (Figure 1b). There are two kinds of copper atoms, Cu(1) and Cu(2), both having distorted octahedral coordination of oxygen atoms. The MoO_4 tetrahedra connect these chains into a 3D net where the ribbons form a herringbone arrangement when viewed down the ribbon axis.

Each ribbon alternately contains one Cu(1) octahedron and two Cu(2) octahedra, all being edge-shared (Figure 1). The copper octahedra are strongly distorted with a 4 + 2 environment (Tables 3 and S2). For both copper atoms, their environments contain four oxygen atoms from molybdate anions and two hydroxides. While for Cu(1), the OD groups are in trans positions, they are in cis positions for Cu(2). The apical distortion of the copper octahedra is related to a strong Jahn−Teller effect (Figure 1a). The distortion is more symmetric for Cu(1) with two equal apical bonds, 2.409 Å, and a mean equatorial bond length of 1.985 Å because Cu(1) lies on a center of symmetry. For Cu(2), the corresponding bond lengths are 2.306 and 2.476 Å for the apical ones and 1.962 Å for the mean equatorial value. These distortions are also seen in the angles that range from 73 to 99° and from 155 to 180° for O−Cu−O.

The MoO_4 plays an important role in the structure, as does the SO_4 in the metal−hydroxy sulfates.[2] It connects three ribbons together (Figure 2) via its oxygen atoms: O(1) and O(3) are bonded to single Cu atoms, while O(2) and O(4) bridges two copper atoms each on two adjacent chains. The latter oxygen atoms are also part of the skeleton of the ribbons. The MoO_4 shares its oxygen corners with six copper atoms defining a μ_6 environment. The MoO_4 tetrahedron is slightly distorted (Tables 3 and S2) with Mo−O bond lengths between 1.754 and 1.774 Å (mean value 1.765 Å) and angles between 108.1 and 111.7°. Its deformation from a regular tetrahedron is less pronounced compared to the X-ray results of Hawthorne and Eby.[14]

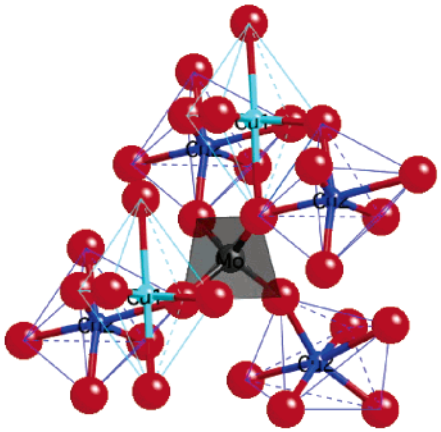

Figure 2. The μ_6-mode of coordination of the MoO_4 unit to its three neighboring ribbons of copper hydroxide.

Table 4. Empirical Bond Valence for Lindgrenite[33]

	Cu1	Cu2	Mo	H + D	Σ
O1		0.510(5)	1.489(14)		1.999(15)
O2	0.139(1) (×2)	0.184(2)	1.511(14)		1.834(15)
O3		0.502(5)	1.441(15)	0.020(1)	2.018(16)
				0.055(1)	
O4	0.477(4) (×2)	0.116(1)	1.434(15)		2.026(15)
OD	0.403(3) (×2)	0.436(5)		0.060(3)	2.163(14)
		0.422(4)		0.842(3)	
Σ	2.036(7)	2.169(10)	5.875(29)	0.977(3)	

The O−D bond length is 0.956(4) Å, and the group is involved in one deuterium bond with O3, D−O3 = 1.966(4) Å and OD−D−O3 = 150.3(5)°. The oxygen atoms exhibit μ_2 (O1 and O3) and μ_3 (O2, O4, OD) environments.

Finally, calculation of the bond valences (Table 4) according to the model of Altermatt and Brown yields values in agreement with the expected ones.[33] The agreement is even better than for the corresponding values calculated from the X-ray single-crystal data of Hawthorne and Eby.[14] This is particularly true for the O4 atom where the sum of individual bond valences decreases from 2.53 to 2.026.

Magnetic Properties. The magnetic properties of the two compounds $Cu_3(OH)_2(MoO_4)_2$ (**1**) and $Cu_3(OD)_2(MoO_4)_2$ (**2**) are very similar, and here, we report those of the purer of the two, $Cu_3(OH)_2(MoO_4)_2$ (**1**). The magnetic susceptibility measured in an applied field of 100 Oe is shown in Figure 3 as $1/\chi$ and χT. From 300 to 30 K, χT decreases gradually

(33) (a) Altermatt, D.; Brown, I. D. *Acta Crystallogr.* **1985**, *B41*, 240−244. (b) Brown, I. D.; Altermatt, D. *Acta Crystallogr.* **1985**, *B41*, 244−247.
(34) Kurmoo, M.; Kumagai, H.; Akita-Tanaka, M.; Inoue, K.; Takagi, S. *Inorg. Chem.* **2006**, *45*, 1627 and references therein.
(35) Bertaut, F. *Acta Crystallogr.* **1968**, *A24*, 217.
(36) (a) Hovestreydt, E.; Aroyo, I.; Sattler, S.; Wondratschek, H. KAREP—A program for calculating irreductible space group representations. *J. Appl. Crystallogr.* **1992**, *25*, 544. (b) Rodriguez-Carvajal, J. *BASIREPS—A program for calculating non-normalized basis functions of the irreductible representations of the little group Gk for atom properties in a crystal*; Laboratoire Léon Brillouin (CEA-CNRS): CEA Saclay, Gif sur Yvette, France.

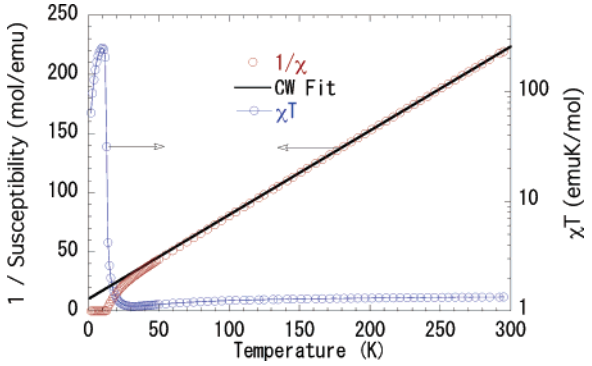

Figure 3. Temperature dependence of the inverse magnetic susceptibility (red circles) and of effective moment represented as χT (blue circles). The black solid line is the least-square best fit to the Curie−Weiss law.

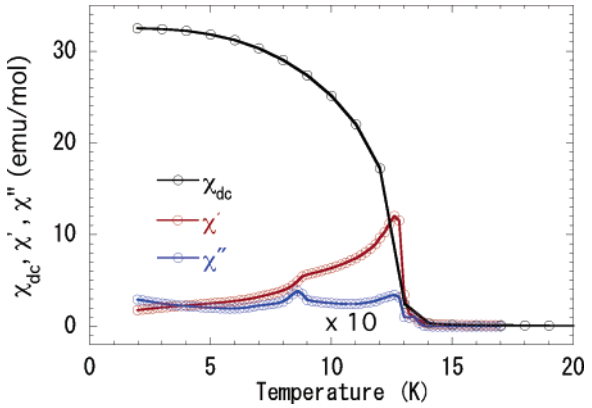

Figure 4. Temperature dependence of the dc and ac magnetic susceptibilities.

to a shallow minimum before a sharp increase, reaching a maximum at 10 K. In the temperature range of 100−300 K, the magnetic susceptibility follows the Curie−Weiss law, $\chi = C/(T - \theta)$, with the Curie constant of $C = 1.406(1)$ emu mol^{-1} and the Weiss temperature of $\theta = -14.2(2)$ K. Using $C = Ng^2\mu_B{}^2S(S + 1)/3k$ and $S = 1/2$ for Cu^{2+}, we obtain $g = 2.236(1)$, which is in fair agreement with the values in the literature. The negative Weiss temperature suggests the dominance of antiferromagnetic near-neighbor interaction. Below 28 K, the χT product starts to increase, first progressively and then steeply between 13 and 12 K to reach a maximum at 10 K. At lower temperatures, χ reaches a plateau, whereas χT decreases. The ac-susceptibility measurements reveal the presence of a peak on both the real and imaginary components with a maximum of χ' at 12.6 K (Figure 4), signaling the presence of a long-range magnetic ordering. It is worth noting that the degree of frustration (f),[37c] estimated by the ratio of the Weiss temperature (θ) to the Curie or Néel temperature (T_C or T_N), is almost unity. This may then be regarded as being close to the mean field, but in the presence of both ferromagnetic and antiferromagnetic exchanges, it cannot be the case (see later). A second anomaly is also detected at around 8 K. Isothermal magnetization at different temperatures (Figure 5) were recorded

(37) (a) Riuz, E; Cano, J.; Alvarez, S.; Alemany, P. *J. Am. Chem. Soc.* **1998**, *120*, 11122. (b) Weihe, H.; Güdel. H. U. *J. Am. Chem. Soc.* **1997**, *119*, 6539. (c) Weihe, H.; Güdel, H. U. *J. Am. Chem. Soc.* **1998**, *120*, 2870. (d) Weihe, H.; Güdel, H. U. *Inorg. Chem.* **1997**, *36*, 3632.

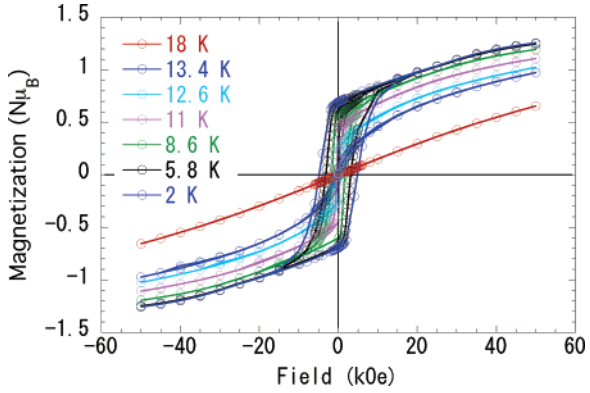

Figure 5. Isothermal magnetization at different temperatures.

to shed some light on the latter anomaly. First, we observe a paramagnetic behavior above (18 K) the Curie temperature and superparamagnetic just above (13.4 K). At 12.6 K, there is a small hysteresis loop with a very weak coercive field. As the temperature is lowered further, a prominent square shape hysteresis loop develops whose coercive field and remanant magnetization increase (Figures S5 and S6). The magnetization reaches a value of 1.256 N μ_B mol^{-1} (0.42 N μ_B mol^{-1} of Cu) at 2 K in the maximum field. Therefore, all the results (minimum in χT, negative Weiss temperature, and saturation magnetization of nearly 1/3 of the expected total) are consistent with those expected for a topological ferrimagnetic chain differing in the number of equivalent moments in the two sublattices.[34] In addition, the sharp anomalies at 12.6 K in the ac susceptibilities confirm the long-range ordering to be ferrimagnetic. One unusual observation is the constant increase of the saturation magnetization without a change in slope of the magnetization as a function of field (>20 kOe) for all temperatures below T_C. The value of the saturation magnetization, of nearly 1/3 of the total moment, is close to that expected for one resultant copper moment. However, the hysteresis loop measurements in the temperature range, where the second anomaly at 8 K was observed in the ac-susceptibility data, do not reveal any change in the evolution. It is to be noted that there is a decrease in the real part of the ac susceptibilities, suggesting that the anomaly cannot be the presence of an impurity. A magnetic impurity is expected to add a component to the total. One plausible explanation is a change of magnetic hardness or relaxation intrinsic to the low-dimensional nature of the compound. Consequently, the anomaly is not seen in the dc magnetization. With the exception of the ac susceptibilities and the isothermal magnetization at different temperatures that were not reported by Shores et al., all our results are in good agreement.[10]

Specific Heat. To get more insight of the magnetic ordering for this material, the specific heat measurements in zero-field were performed. Figure 6 shows the experimental temperature dependence of the temperature-normalized heat capacity corrected for the lattice phonons as follows: $C_m = C_p - C_{lattice}$, where the lattice contribution is expressed by $C_{lattice} = \beta_1 T^3 +$ higher terms (higher terms are assumed to be very small in our case because of the

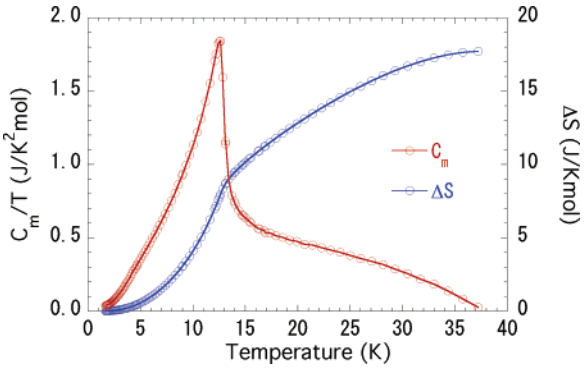

Figure 6. Temperature dependence of magnetic heat capacity normalized to the temperature (experimental data in red circles) and the corresponding integrated entropies (blue circles). Lines are a guide for the eyes.

limited temperature range of the measurements) and β_1 is related to the Debye temperature.

The magnetic heat capacity normalized by the temperature shows a λ anomaly, peaking at 12.6 K, at the long-range magnetic ordering discussed above. The magnetic entropy was obtained by integrating the C_m/T versus T curve within the limit of the experimental temperature range (assuming the heat capacity is zero at 0 K). The value of the total entropy up to 37 K of 17.7 J K^{-1} mol^{-1} is close to that expected for three copper atoms, $3R$ ln($2S + 1$), of 17.3 J K^{-1} mol^{-1} for $S = 1/2$. Of this total, only 50% is accounted for below the Curie temperature. The remaining entropy is, therefore, associated with the short-range correlation resulting from the low-dimensionality of the system. Again no unusual behavior is observed at 8 K. The fact that (a) there is a well-defined λ-peak in the heat capacity data at the long-range magnetic ordering temperature, (b) the heat capacity tends toward zero as the temperature moves toward zero, and (c) the estimated magnetic entropy is as expected rules out the presence any geometry-associated magnetic frustration. This agrees with the frustration factor of unity from the magnetic data discussed above.

Magnetic Structure. A comparison of the diffractograms ($\lambda = 2.4266$ Å) recorded at 1.5 and 17.8 K reveals only slight differences as expected for the low moment of copper. No new lines appear, and one observes principally an enhancement in the intensity of the line at $2\theta = 27.17°$, indexed as (0 1 1) (Figures S7 and S8). The same observation is made for the (−1 0 1) line at 33.73°. These Bragg angles of the difference peaks are consistent for all temperatures below the long-range magnetic ordering suggesting a commensurate $k = (0\ 0\ 0)$ propagation vector. In the difference pattern, the intensities of few other lines increase very slightly at low temperature. Among them, one notices the (0 4 0) at 40.35° and a weaker one (0 0 2) at 51.83°. Such behavior is usually characteristic of a ferromagnetic structure since all the magnetic scatterings appear at the same angles as those of the nuclear ones. The fact that the (0 4 0) and (0 0 2) lines have each a magnetic contribution suggests the most possible orientation of the magnetic moments is along the *a* axis. To solve the magnetic structure, we determined the associated magnetic structure with the help of Bertaut's representation analysis method,[35] applied to $P2_1/n$ space group, $k = (0\ 0\ 0)$ propagation vector, and 2a and 4e Wyckoff positions for the Cu1 and Cu2 copper ions, respectively. Four one-dimensional irreducible representations (IR), $\Gamma_1-\Gamma_4$, are associated to basis vectors (magnetic structures) for Cu2, while only two, Γ_2 and Γ_4 (Table 5), are associated with Cu1.[36] Therefore, only the latter two need to be considered as possible models. In the first one, the moments are along the *b* axis; in the second one, they are in the *ac* plane. Both representations have been checked by considering that the Cu1 and Cu2 magnetic moments are either independent or equal. As expected, the best refinement (Figure 7) is obtained for the Γ_4 representation with the magnetic moments oriented along the *a* axis, with opposite orientation of moments for Cu(1) and Cu(2). The refinement performed for independent moments of the two copper atoms was of lower certainty compared to those for equal moments. On the other hand, a model with moments along the *b* axis is less reliable (Table 6).

From this table, it appears that the best model corresponds to magnetic moments along the *a* axis with equal values for

Table 5. Basis Functions of the Irreducible Representations, Γ_2 and Γ_4[a]

IR	moment	Cu11	Cu12	Cu21	Cu22	Cu23	Cu24
Γ_2	M_x, M_y, M_z	+ + +	− + −	+ + +	+ + +	− + −	− + −
Γ_4	M_x, M_y, M_z	+ + +	+ − +	+ + +	+ + +	+ − +	+ − +

[a] Cu11 (0, 0, 0); Cu12 (1/2, 1/2, 1/2); Cu21 (x, y, z); Cu22 ($-x$, $-y$, $-z$); Cu23 ($1/2 - x$, $1/2 + y$, $1/2 - z$); Cu24 ($1/2 + x$, $1/2 - y$, $1/2 + z$).

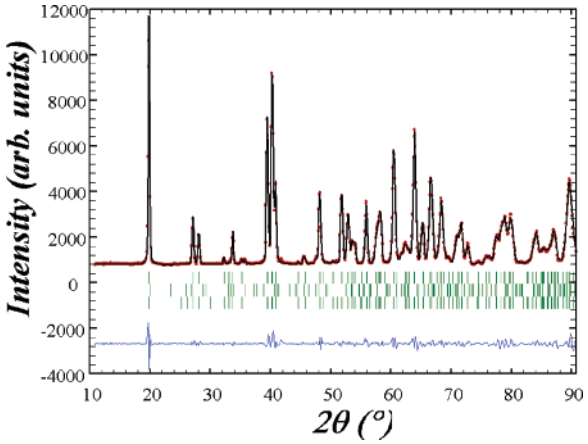

Figure 7. Observed (circles) and calculated (line) profiles of the neutron powder diffraction pattern of $Cu_3(OD)_2(MoO_4)_2$ obtained on the G4.1 diffractometer ($\lambda = 2.4266$ Å) at 1.5 K with position of the Bragg reflections (short vertical lines) of $Cu_3(OD)_2(MoO_4)_2$ and of $Na_2MoO_4 \cdot D_2O$ and difference between observed and calculated profiles.

Table 6. Results of the Refinements

moment orientation	copper ion	M_x (μ_B)	M_y (μ_B)	$R_{magnetic}$
a axis	Cu1	0.83(30)	0[a]	5.45%
	Cu2	−0.78(19)	0[a]	
a axis	Cu1	0.77(4)	0[a]	4.90%
	Cu2	−0.77(4)	0[a]	
b axis	Cu1	0[a]	0.81(26)	6.38%
	Cu2	0[a]	−0.77(16)	
b axis	Cu1	0[a]	0.79(4)	6.33%
	Cu2	0[a]	−0.79(4)	

[a] The moments are significantly lower than their corresponding standard deviations. The same is true for the M_z component for all models.

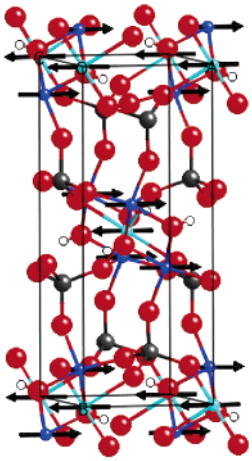

Figure 8. Alignment of the magnetic moments in the magnetic structure of $Cu_3(OH)_2(MoO_4)_2$ below 12 K.

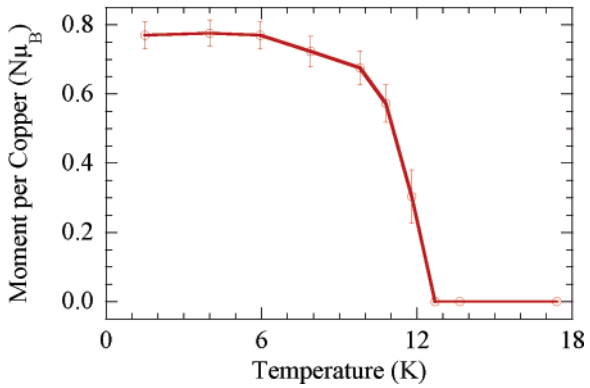

Figure 9. Temperature dependence of the magnetic moment per copper.

both Cu1 and Cu2. The presence of a magnetic contribution on the (0 4 0) line certainly confirms this model. Figure 7 shows the observed and calculated diffraction patterns. The magnetic structure of lindgrenite is that of a topological ferrimagnet (Figure 8) with magnetic moments aligned along the *a* axis for Cu(1) and in the opposite one for Cu(2) and the moment value being 0.77(4) μ_B at 1.5 K (Figure 9). The same model also applies for all the temperatures below T_C, and the thermal evolution of the magnetic moments is given in Figure 9. The magnetic moment value is nearly constant between 1.5 and 8 K and starts to decrease at 10 K (Table S3). We note that the moment saturates around the temperature where the anomaly is observed in the ac susceptibilities. No other difference is observed in the diffractograms. The fact that the model with equal moments gives rise to a better fit is because the two copper atoms have similar coordination geometry. It is also worth noting the absence of any broad diffraction and enhanced scattering at small angles at all temperatures, above and below the long-range magnetic ordering; this may indicate the presence of frustration or short-range clustering of moments.[2]

It is of interest to understand why lindgrenite orders as a ferrimagnet by searching for any existing structural correlation. For this 3D structure, there are two crystallographically independent copper atoms, namely, Cu(1) and Cu(2), where there are one Cu(1) and two Cu(2) in a unit belonging to a ribbon. Cu(1) sits on an inversion center. The unit cell contains two of Cu(1) and four of Cu(2) belonging to a central ribbon and four near neighbor ones. The closest Cu−Cu distance (3.01−3.21 Å, Table S2) is via one-oxygen-atom bridges where the oxygen is either the OH, O(2), or O(4) of MoO_4. These provide the major magnetic interaction pathways. Because of the three different bond-distances and the Cu−O−Cu angles, one can define three independent interactions. Consequently, the expected degeneracy arising from geometrical frustration of an equilateral triangular system of $S = 1/2$ can be lifted. Assuming the results of existing theoretical calculations that for an angle less than 98° a ferromagnetic exchange is favorable and one greater than 98° is antiferromagnetic, we can define both for the nearest-neighbor copper atoms. We note that there are two different angles defining each magnetic pathway (Table S2), and in most cases, one angle is lower than 98° and the other is greater. It is believed that in such cases the AF is the most likely exchange.[37] The next hierarchical exchange interactions are those involving Cu−O−Mo−O−Cu pathways. Here, we can define 13 independent ones, 2 within one ribbon and 11 between ribbons. The MoO_4 units around one ribbon connect six neighboring ribbons. In principle, these are very weak and appear to favor parallel alignment of the corresponding moments on neighboring ribbons. Therefore, they must be weakly ferromagnetic in nature. It is interesting to note that the weak magnetic anisotropy of copper favors a moment perpendicular to the ribbon, while a strong anisotropy (from say Co(II) or Mn(III)) may favor an Ising system with alignment along the ribbons. The above arguments and the results of magnetization and neutron scattering are consistent with a picture where the moments of the two different copper atoms are aligned antiparallel to one another within the ribbons with the resultant moment of each ribbon being parallel to give a ferrimagnet. This is different than the interpretation and proposed mechanism of the magnetization reversal by Shores et al.[10] From the results of our findings, it is worth noting in the work of Shores et al. that introduction of bipyridine or piperazine separates the 3D structure into layers and, consequently, results in an antiferromagnetic ground state, where the weak antiferromagnetic interaction via the ditopic ligands can be switched by a weak magnetic field of 2 kOe to obtain the ferrimagnetic ground state of the parent lindgrenite. Although the fitting of high-temperature magnetic susceptibility data for compounds having bpy bridges suggest that exchange through the bpy ligand is zero,[38] the data of Shores et al.[10] and those of more recent studies[39] show that exchange through bpy is present but may be small. In contrast, a different picture emerges for the presence of the more anisotropic Co^{2+} in $Co_3(OH)_2(C_4O_4)_2 \cdot 3H_2O$,[15] where each ribbon is ferromagnetic and the moments on adjacent ribbons are antiparallel, thus resulting in a LRO Néel ground state in a small field. The application of a high

(38) Julve, M.; Verdaguer, M.; Faus, J.; Tinti, F.; Moratal, J.; Monge, A.; Gutiérrez-Puebla, E. *Inorg. Chem.* **1987**, *26*, 3520.
(39) (a) Wang, X-Y.; Wei, H-Y.; Wang, Z-M.; Chen, Z-D.; Gao, S. *Inorg. Chem.* **2005**, *44*, 572−583. (b) Feyerherm, R.; Loose, A.; Lawandy, M. A.; Li, *J. Appl. Phys. A* **2002**, *74* (Suppl., Part 1), S778−S780. (c) Feyerherm, R.; Loose, A.; Lawandy, M. A.; Li, J. *Phys. Chem. Solids* **2002**, *63*, 71−77.

field reverses the moment easily to the ferromagnetic state. Furthermore, removal of the occluded water molecules in the channels also results in a ferromagnetic state. This process is reversible. The results of these works highlight the importance of weak magnetic exchange through large organic bridges or hydrogen bonds that can transform these materials between different ground states.

Conclusion

$Cu_3(OH)_2(MoO_4)_2$ and $Cu_3(OD)_2(MoO_4)_2$, prepared at moderately low temperatures in the laboratory, are isostructural to the mineral lindgrenite. The magnetic properties are consistent with those of a ferrimagnet with a Curie temperature (T_C) of 13 K with reasonable magnetic hardness with complete absence of geometrical frustration. The heat capacity gives only 50% of the entropy below T_C, and the remaining amount is taken up by the low dimensionality. Below T_C, the magnetic structure refined from neutron diffraction data presents ferrimagnetic ribbons with parallel resultant moments. The distortion of the $Cu_3(OH)$ unit from being an equilateral triangle appears to lift the degeneracy in the spectrum, thus resulting in an ordered state without spin frustration.[40] Using the present result from the neutron data analyses of the parent lindgrenite, we were able to propose a different model to explain the magnetic properties of the bipyridine-functionalized lindgrenite.[10]

Acknowledgment. We gratefully acknowledge the CNRS for funding.

Supporting Information Available: Infrared, DT-TGA, nuclear and magnetic crystallographic (tables of bond lengths and angles), and magnetic data for compounds **1** and **2**. This material is available free of charge via the Internet at http://pubs.acs.org.

IC061182M

(40) (a) Bramwell, S. T.; Gingras, M. J. P. *Science* **2001**, *94*, 1495. (b) Greedan, J. E. *J. Mater. Chem.* **2001**, *11*, 37. (c) Ramirez, A. P. In *Handbook of Magnetic Materials*; Buschow, K. J. H., Ed.; Elsevier Science: Amsterdam, 2001; Vol. 13, p 423. (d) Grohol, D.; Matan, K.; Cho, J.-H.; Lee, S.-H.; Lynn, J. W.; Nocera, D. G.; Lee, Y. S. *Nat. Mater.* **2005**, *4*, 323. (e) Diep, H. T., Ed. *Magnetic Systems with Competing Interactions: Frustrated Spin Systems*; World Scientific: Singapore, 1994.